Received: 8 November 2023 | Revised: 26 February 2024 | Accepted: 31 March 2024

DOI: 10.1111/jace.19849

Journal of the American Ceramic Society

RESEARCH ARTICLE

Microplastic response of 2PP-printed ceramics

Johanna C. Sänger[1,2] | **Birte Riechers**[2] | **Brian R. Pauw**[2] | **Robert Maaß**[2,3,4] | **Jens Günster**[2,5]

[1]Chair of Structural and Functional Ceramics, Department of Materials Science, Montanuniversität Leoben, Leoben, Austria

[2]Federal Institute for Materials Research and Testing (BAM), Berlin, Germany

[3]Department of Materials Science and Engineering, University of Illinois at Urbana-Champaign, Urbana, Illinois, USA

[4]Department of Materials Engineering, Technical University of Munich, Garchingen, Germany

[5]Institute of Non-Metallic Materials, Clausthal University of Technology, Clausthal-Zellerfeld, Germany

Correspondence
Johanna C. Sänger and Jens Günster, Federal Institute for Materials Research and Testing (BAM), 12205 Berlin, Germany.
Email: Johanna.Saenger@bam.de and Jens.Guenster@bam.de

Funding information
HORIZON EUROPE European Innovation Council, Grant/Award Number: 101063523; Bundesanstalt für Materialforschung und -Prüfung

Abstract

Two-photon polymerization (2PP) additive manufacturing (AM) utilizes feedstocks of ceramic nanoparticles of a few nanometers in diameter, enabling the fabrication of highly accurate technical ceramic design with structural details as small as 500 nm. The performance of these materials is expected to differ from conventional AM ceramics, as nanoparticles and three-dimensional printing at high resolution introduce new microstructural aspects. This study applies 2PP-AM of yttria-stabilized zirconia to investigate the mechanical response behavior under compressive load, probing the influence of smallest structural units induced by the line packing during the printing process, design of sintered microblocks, and sintering temperature and thereby microstructure. We find a dissipative mechanical response enhanced by sintering at lower temperatures than conventional. The pursued 2PP-AM approach yields a microstructured material with an increased number of grain boundaries that proposedly play a major role in facilitating energy dissipation within the here printed ceramic material. This microplastic response is further triggered by the filigree structures induced by hollow line packing at the order of the critical defect size of ceramics. Together, these unique aspects made accessible by the 2PP-AM approach contribute to a heterogeneous nano- and microstructure, and hint toward opportunities for tailoring the mechanical response in future ceramic applications.

KEYWORDS
additive manufacturing, mechanical properties, microstructure, plasticity, zirconia: yttria stabilized

1 | INTRODUCTION

Additive manufacturing (AM) promises to transfer the unique properties of advanced ceramics to applications via novel designs and shapes.[1] A conventional route in ceramics production is the powder processing chain,[2] where AM serves as a shaping technology to obtain ceramic powder compacts that yield fully dense ceramics after the sintering process. It is specifically the high density after sintering, typically >99% of the theoretical density (TD), that enables the unique physicochemical properties that ceramic materials are so well-known for.[3]

Over the past years, novel AM technologies were developed involving feedstocks of slurries. They are designed to improve the powder bed density during the printing process and with that the density and integrity of the final ceramic compound. Water-based slurries are favorable for manufacturing of voluminous parts,[4,5] while organic-based slurries, including photocurable resins, are advantageous to manufacture filigree structures.[6] Of particular interest are slurry recipes suitable for two-photon polymerization (2PP) that use yttria-stabilized zirconia (YSZ) ceramic nanoparticles, thus ensuring high transparency in the visual spectrum.[7] The very small particle size of about 5 nm, which is well below typical particle sizes for the powder processing chain of 20 nm to 400 μm,[8,9] leads to a unique enhanced sintering activity of the 2PP-slurry.[10,11] For example, bulk zirconia powders with larger particle size are typically sintered between 1350°C and 1500°C,[12] whereas sintering of 2PP-slurries with zirconia nanoparticles required significantly lower temperatures to achieve near-bulk densities. Similarly when sintered at corresponding high bulk powder sintering temperatures, the nanoparticles in the as-printed 2PP-structure undergo extended grain growth that leads to self-healing to a certain extent, but which decreases the printing resolution.[7] Moreover, mechanical compression testing demonstrated strength levels for 2PP-zirconia ceramics sintered at 1200°C that can compete with bulk zirconia even when printed with designed porosity.[7] These findings indicate a strong benefit from using nanosized particles on the mechanical performance of 2PP-zirconia, underlining earlier results that reveal access to favorable transgranular fracture modes and grain-boundary reinforcements with decreasing particle size as shown for Al_2O_3.[13]

A major advantage of 2PP-AM is the ability to construct geometries with a resolution and contour accuracy that cannot be achieved with conventional AM technologies. This allows for accessing very specific designs of hollow and filigree structures such as triple periodic minimal surfaces. These structures show uniform stress distributions and therefore good mechanical strength at high porosity, which in the case of soft-matter printing suits, for example, tissue engineering applications.[14] A prominent example for such minimal-surface geometries is the SchwarzP design,[15] showing good mechanical properties while only consisting of 56% of the material used for a monolithic design. In fact, 2PP-AM now allows to transfer these design concepts to zirconia ceramics with internal structural fillings at a resolution limit of 500 nm.[7] This design approach combined with the marked increase in grain-boundary volume in such 2PP-AM ceramics prompts the hypothesis that ceramic microstructures are in reach that potentially allow enhanced structural dissipation over conventional bulk ceramics. If corrected, fundamental questions related to structural-design optimization and microplastic processes in the ceramics emerge.

To this end, we investigate here the quasistatic and dynamic mechanical response of monolithic and SchwarzP designs with varying porosity and sintered at different temperatures. Our results reveal a pronounced mechanical dissipation in 2PP-AM YSZ structures that is inverse proportional to the packing density. This microplastic signature is discussed in terms of varying grain sizes and ligament dimensions across the probed structure and show how sintering conditions and structural design can introduce mechanical dissipation in 2PP-AM ceramics.

2 | EXPERIMENTAL PROCEDURES

The feedstock for the 2PP-process contains 70 wt% of 5 nm YSZ nanoparticles (nanoBinder, CeraNovis GmbH) characterized by small-angle X-ray scattering (SAXS) and transmission electron microscopy (TEM). The photocurable matrix consists of poly(ethylene glycol) diacrylate (PEGDA; average M_n = 250, Sigma-Aldrich) with 2,5-bis[4-[N,Nbis-[2-(acetyloxy)ethyl]phenyl]-methylene]-(2E,5E)-cyclopentanone (BAE, Genosynth) and 2,2-dimethoxy-2-phenylacetophenon (DMPA, Sigma-Aldrich) serving as 2PP and ultraviolet (UV)-photoinitiator, respectively. To ensure reproducible printing accuracy, the usage of the feedstock is limited to 3 months after its production due to the tendency of photopolymer degradation.

Two different designs of ceramic microblocks, SchwarzP and cubes, were printed by 2PP in direct contact onto a supportive substrate for facilitated handling. The substrate is prepared from a macroscopic layer of resin, cross-linked by UV radiation prior to the printing of the microblocks.[16] Using different infill line distances for the print of 0.5 and 2 μm creates dense and hollow blocks, respectively. This allows for testing the influence of designed porosity at this high volumetric resolution. After laser-assisted printing at a wavelength of 800 nm, the microblocks were sintered at either 1200°C or 1450°C together with the substrate to densify the material from a powder compact with approximately 50% TD to a ceramic of up to approximately 90% TD, showing only subtle distortion. Further details on the fabrication and sintering process for substrate and microblocks are provided elsewhere.[7]

All as-sintered, that is, pristine, and mechanically tested microblocks were assessed visually by means of scanning electron microscopy (SEM, EVO MA10, Carl Zeiss GmbH). To enhance the SEM-imaging conditions and to reduce electron-charging effects, as-sintered microblocks

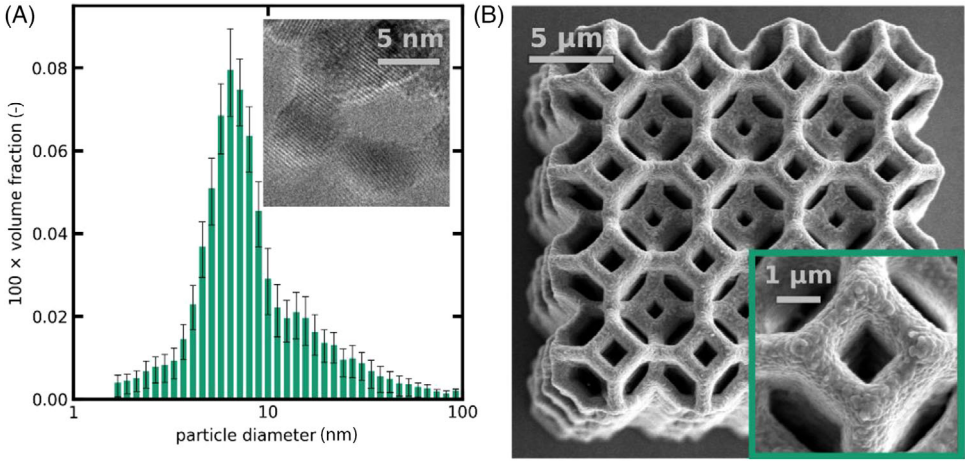

FIGURE 1 (Panel A) Characterization of yttria-stabilized zirconia (YSZ) nanoparticles. Panel A shows the volume-weighted particle size distribution based on a small-angle X-ray scattering measurement of a photocured film of 100 µm thickness with a transmittance of 84% and nanoparticle weight fraction of 4.6%. The inset shows a transmission electron microscopy micrograph of the nanoparticles. Note the resolution visualizing single atomic layers within the YSZ nanoparticles. (Panel B) Three-dimensional lattice cube printed from the transparent resin consisting of up to 80 wt% of the nanoparticles from Panel A. The structure shows the highest achievable accuracy for technical ceramic additive manufacturing of 500 nm. The insert reveals the ceramic character of the structure with typical sintered ceramic grains visible at the surface.

were gold-coated by sputter deposition previous to the SEM analysis. The outer shape of cubic and SchwarzP microblocks before sintering is 40 × 40 × 40 µm^3, which amounts to 25 × 25 × 25 µm^3 and 23 × 23 × 23 µm^3 after sintering at 1200°C and 1450°C, respectively. Of all the realizations of printed microblocks, densely printed and sintered cubes are expected to be most relatable to conventionally produced and sintered YSZ which has a density of 6.03 g/cm^2.[17] From the geometrical dimensions determined by SEM analysis and by assuming perfectly cubic shapes of microblocks, the density can be derived based on the amount of material consumed in the printing process. With these assumptions, densities of 4.4 g/cm^2 and 5.7 g/cm^2 are obtained for dense cubes sintered at 1200°C and 1450°C, respectively, corresponding to up to 94.5% of the density of conventionally produced and sintered YSZ.

Mechanical compression testing of ceramic microblocks was performed using a Hysitron TI-980 Triboindenter equipped with a high-load OmniProbe transducer from Bruker using a flat-punch tip of 100 µm in diameter under ambient conditions. Mechanical tests were performed under load control at a constant loading rate of 0.1 N/s, following a three-stage protocol. First, a linear increase in load was applied up to 600 mN. This is followed by a cyclic load section consisting of linear loading and unloading by 50 mN around 600 mN at a rate of 0.1 N/s, corresponding to a period time of 1 s and 600 consecutive zigzag periods. Finally, the load is linearly reduced at a rate of −0.1 N/s.

3 | RESULTS

A critical aspect for reproducibility and homogeneity in printing the here presented 2PP-AM ceramic YSZ-microblocks is the quality of the nanoparticles in regard to their particle size distribution, mean particle size, and suspension stability as these define the slurry in terms of transparency, homogeneity, and achievable weight fraction. Figure 1A shows a plot of the particle size distribution exhibiting a maximum at a particle diameter of approximately 5 nm, which is also dominant in TEM micrographs (cf. inset of Figure 1A). Moreover, 99% of the volume fraction are connected to particles of less than 80 nm in diameter, a length scale that corresponds to 10% of the applied laser wavelength. Thus, scattering of the laser light becomes significantly reduced, resulting in a transmittance of up to 95% that allows the production of a photocurable feedstock with up to 80 wt% YSZ nanoparticles.[7] An example of the achievable accuracy is presented by the densely printed lattice cube with a resolution of 1 µm in Figure 1B.

The quasistatic mechanical response of printed microblocks to an increasing load is presented in Figure 2A. The plot holds two subgroups, corresponding to SchwarzP and cubic microblocks, each of which shows a systematic reduction in the overall steepness of the load–displacement curves with decreasing sintering temperature and, additionally, decreasing line packing. Densely packed SchwarzP and cubic microblocks sintered at 1450°C show almost identical mechanical

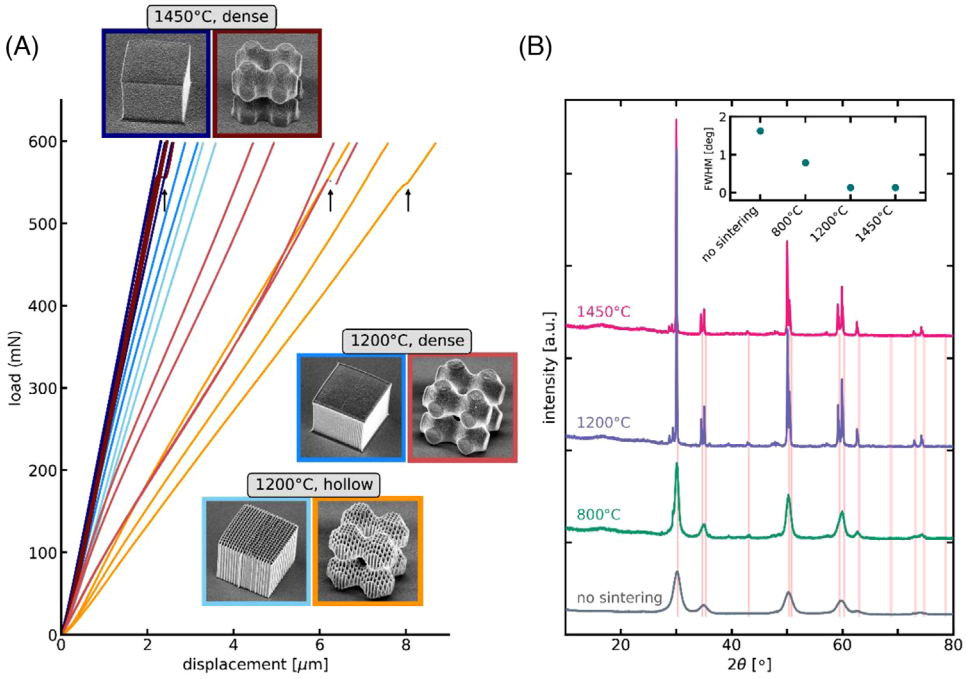

FIGURE 2 (Panel A) Load–displacement curves corresponding to the loading section of mechanical tests on SchwarzP (orange/red) and cubic (blue) microblocks. These were sintered at 1200°C or 1450°C and printed with either dense or hollow line packing. Scanning electron microscopy micrographs show examples of microblocks obtained before mechanical testing, colors indicate block geometry, sintering temperature, and line packing for mechanical data. (Panel B) X-ray diffractograms for nanoparticles before and after sintering at temperatures as indicated in the plot. Diffraction peaks of tetragonal zirconia phase are indicated by vertical red lines. Data were shifted along the *y*-axis for clarity. Inset: Evolution of the full width at half maximum of diffraction peaks at $2\theta = 30°$ based on sintering conditions.

responses, regardless of differences in design and contact area between tip and top surface of the microblocks. However, the mechanical behavior is clearly different for SchwarzP and cubic microblocks sintered at 1200°C. Now, both SchwarzP-types, of dense and hollow line packing, are more compliant than the corresponding cubic microblocks, indicating an influence by both structural design and line packing after low-temperature sintering. Since this applies to identical geometries but different fully dense microstructures due to the variation in sintering temperatures, displacement (strain) admitting processes must be at place.

Furthermore, the load–displacement curves of the dense microblocks sintered at 1200°C reveal noticeable deviations away from a linearity, which could be ascribed to imperfect testing boundary conditions or originate from microplastic processes occurring in the material at this point. As we will show later, dynamical loading information will support the view of microplastic dissipation, which we here understand as signatures of plastic dissipation without any extensive strain accumulation after a well-defined elastic-to-plastic transition. This is justified by the lack of any global yielding of the curves in Figure 2A. Additionally, pronounced local yielding occurs, which emerges as abrupt steps in displacement. These events are marked with arrows in Figure 2A.

X-ray diffractograms (XRDs) of nanoparticles before and after sintering at 800°C, 1200°C, and 1450°C are shown in Figure 2B. All emerging peaks are connected to the tetragonal phase of YSZ. With increasing sintering temperature, the observed peaks become sharper (cf. inset in Figure 2B), which indicates an increase in the average grain size with increasing sintering temperature.[18]

Indications for local dissipation are found in the SEM micrographs in Figure 3, showing surfaces of microblocks before and after mechanical testing up to 600 mN. Here, the pristine features of SchwarzP microblocks depend clearly on sintering temperature. While the pristine SchwarzP microblocks sintered at 1450°C (Figure 3A) consist of grains of some hundred nanometers with a mostly homogeneous surface, heat treatment at 1200°C (Figure 3C) yields grains of substantially smaller size at about 100 nm with a more heterogeneous surface, akin to the primary 5 nm particles of the slurry. This observation of smaller grain size connected to lower sintering temperatures is in line with the peak broadening in the XRD results from Figure 2B. Upon indentation with the flat-punch tip, the microblocks' structure seems to be further densified as material is shifted toward existing

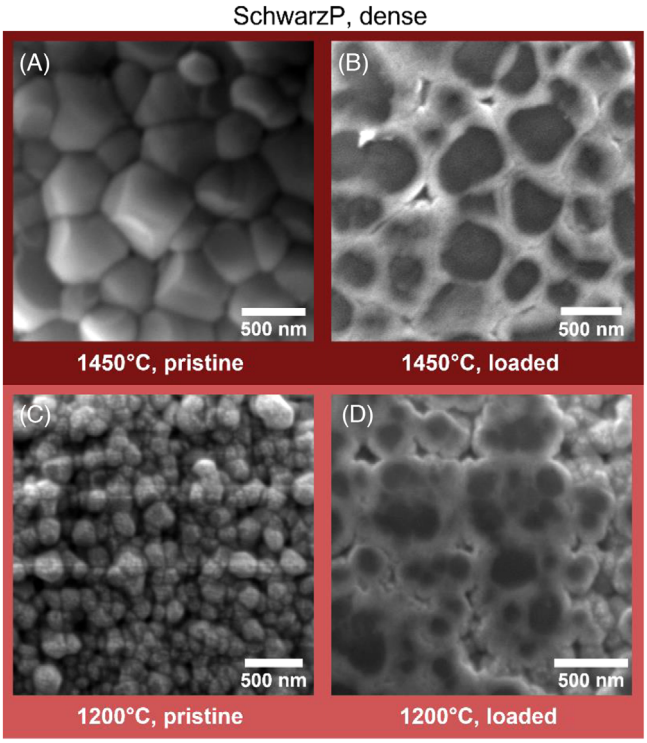

FIGURE 3 Scanning electron microscopy micrographs of densely packed SchwarzP microblocks, sintered at 1450°C before (A) and after (B) mechanical loading, and sintered at 1200°C before (C) and after (D) mechanical loading.

cavities, thus flattened out features in Figure 3B,D give rationale to the more mechanically compliant material behavior observed in Figure 2.

The load imposed onto a SchwarzP microblock during mechanical experiments is distributed over a smaller area than for a cube. Under ideal contact conditions, it corresponds to its four main pillars, amounting to only 20% of the projected load-bearing surface provided by the cubic design. However, SEM micrographs indicate that the experimental situation is more complex as the load is not necessarily evenly distributed over the four pillars of a SchwarzP microblock. This is a typical feature of such small-scale mechanical tests. The tilt between flat punch and specimen results in a nonhomogeneous introduction of load resulting in excessive stresses at positions of highest topography, as evident from inhomogeneous surface densification in Figure 4A,D across the microblocks.

Based on the load–displacement data in Figure 2A, line density has an important influence on the mechanical performance. Figure 4 shows SchwarzP microblocks of dense (Panels A–C) and "hollow" packing, that is, with low line density (Panels D–F). This hollow printing reduces the amount of material by 55% compared to the material needed for a densely packed microblock. The 2PP-printed SchwarzP microblocks show cracks that were initiated where highest stresses occurred, namely, at the lower right pillars (cf. Figure 4B,E). Moreover, plastic deformation is also visible by a nonreversible deformation of all pillar surfaces, as depicted in Figure 3. Interestingly, cracks extend further through the SchwarzP microblock if printed with dense line packing, compared to a more limited crack propagation length observed in hollowly printed microblocks, potentially reducing brittleness. This is a common phenomenon which can be understood as crack deflection by the internal structure of the hollow microblocks.[19] The observed cracks are likely connected to the step-like increases in displacement observed in Figure 2A. Figure 4C,F shows the deformed surfaces of microblocks at higher magnification. Some smaller debris is observed for the densely printed microblock, potentially originating from a disintegration or spalling of the microstructure into single particles at extreme pressure and plastic deformation. High contrast variations could also be a consequence of the gold coating, which was applied to the microblocks for facilitated SEM imaging before mechanical testing. As shown in Figure 4F, the structure of the hollow SchwarzP microblock is strongly densified as well, up to the point where cavities between ligaments are not further visible at the indentation area itself. These observations provide a strong signature of dissipative, possibly microplastic, processes, aligning well with the observations made in Figure 3.

To yield a quantitative measure of any potential plastic dissipation behavior, the material's deformation is measured under application of an oscillatory small-amplitude modulation of the load superimposed with a nominal constant load experiment. In this way, the cyclic load component allows assessing the energy dissipated in the ceramic material during a nominal creep-like response. In Figure 5A, the loading protocol for the cyclic load experiments is plotted, resulting in a concomitant averaged displacement (shown in Figure 5B) observed during this stage. Compared to the trend observed during the quasistatic initial loading segment (Figure 2A), the two different block geometries sintered at 1450°C show the least change in displacement, while microblocks sintered at 1200°C show a stronger increase in displacement over time for cubic microblocks, and strongest changes in displacement for SchwarzP microblocks. The influence from porosity is observed in accordance with previous descriptions but is not sufficiently pronounced to discuss further details regarding the observed absolute amplitudes. The averaged displacement of a Si-wafer is presented together with the microblock data, reflecting the inherent creep compliance of the indentation setup, being well below the microblocks' displacement response.

Next, we focus on the dissipated energy related to the area enclosed within load–displacement cycles in

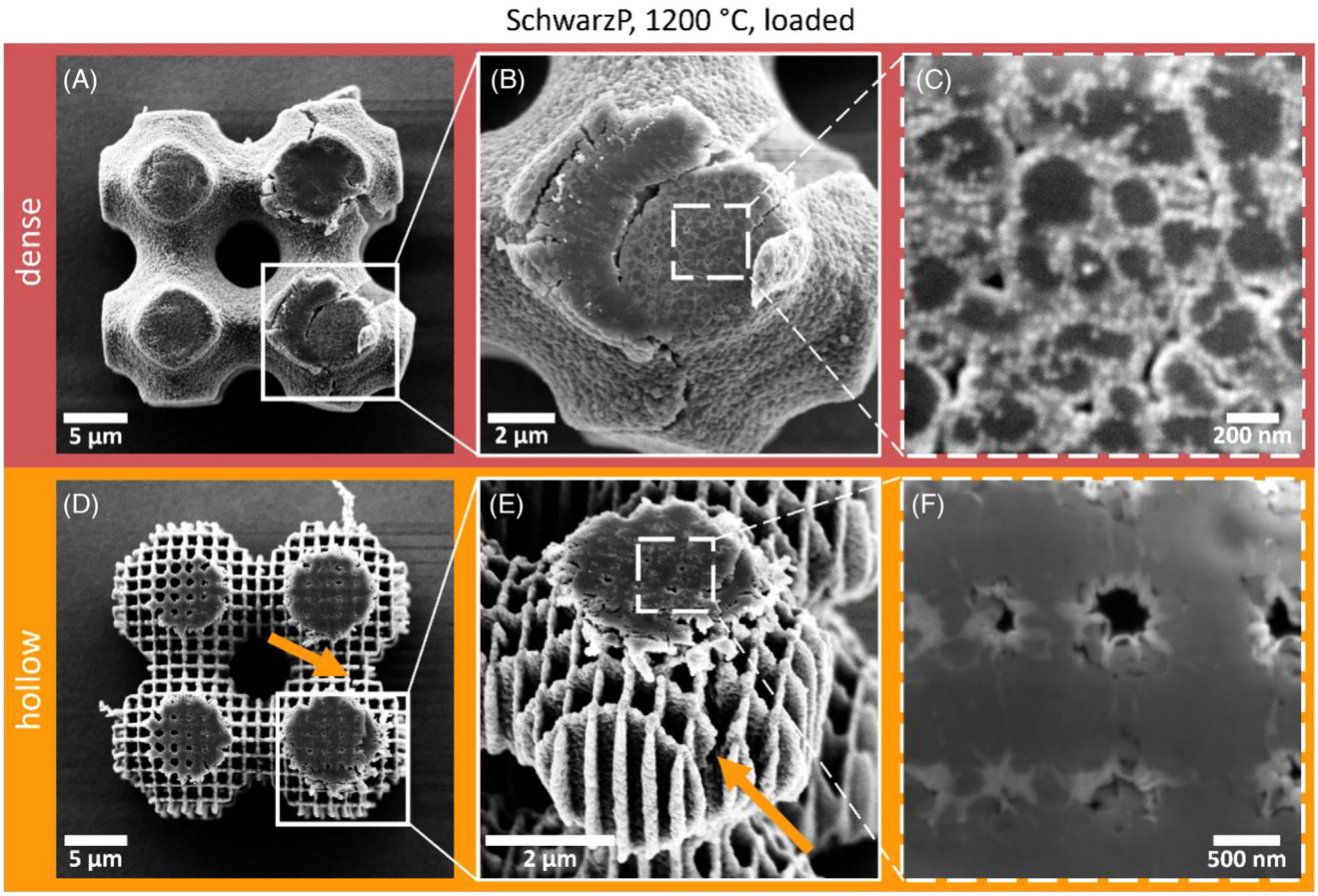

FIGURE 4 Scanning electron microscopy micrographs of mechanically loaded SchwarzP microblocks sintered at 1200°C with dense (A–C) and hollow (D–F) line packing at increasing magnification. Arrows indicate the location of cracks within the hollow SchwarzP microblocks.

Figure 5C where the 20 final cycles of the hold segment are plotted for all tested microblocks after subtracting the linearly fitted slope determined from Figure 5B. This procedure leads to a collapse of the cyclic load–displacement data with quite systematic behavior in regard to the width of the cycles' envelopes. The magnification in Figure 5D shows how this envelope is most narrow for the blocks sintered at 1450°C and becomes wider for microblocks sintered at 1200°C. A quantitative measure for the dissipated energy is provided by assessing the enclosed area, which is obtained by integrating the area under the upper and lower data of a cycle and subsequent subtraction. The results in form of the mean over the final 20 cycles together with the standard deviation are plotted in Figure 5E, which yields a very clear picture on the systematic evolution of dissipated energy based on microblock design, sintering temperature, and line packing. Microblocks sintered at 1450°C show lowest values of dissipated energy at about 1.2 µJ, while a decrease in sintering temperature to 1200°C leads to an increase in the dissipated energy for both cubic and SchwarzP microblocks. For cubic microblocks, however, this increase remains small at about 1.4 µJ for dense and 1.9 µJ for hollow cubes. SchwarzP microblocks exhibit significantly higher dissipation with 2.3 µJ for dense and 3.6 µJ for hollow microblocks. To ensure that the here measured dissipative energies are indeed beyond the resolution limit of the testing setup, an identical load protocol was applied to a Si-wafer mounted in comparable fashion, which yields a system resolution of 5–10 nJ. Thus, the dissipative energies derived here are indeed connected to sample-specific properties and dissipative processes induced within the 2PP-AM ceramic material.

4 | DISCUSSION

As indicated by the nonlinear quasistatic loading behavior and sintering-dependent displacement accommodation, dynamical mechanical testing reveals clear indications for the presence of dissipative microplastic processes in 2PP-AM zirconia-based microstructured ceramics sintered from nanoparticles. The most pronounced mechanical dissipation is observed for material sintered at lower temperature (1200°C) and with high porosity (hollow

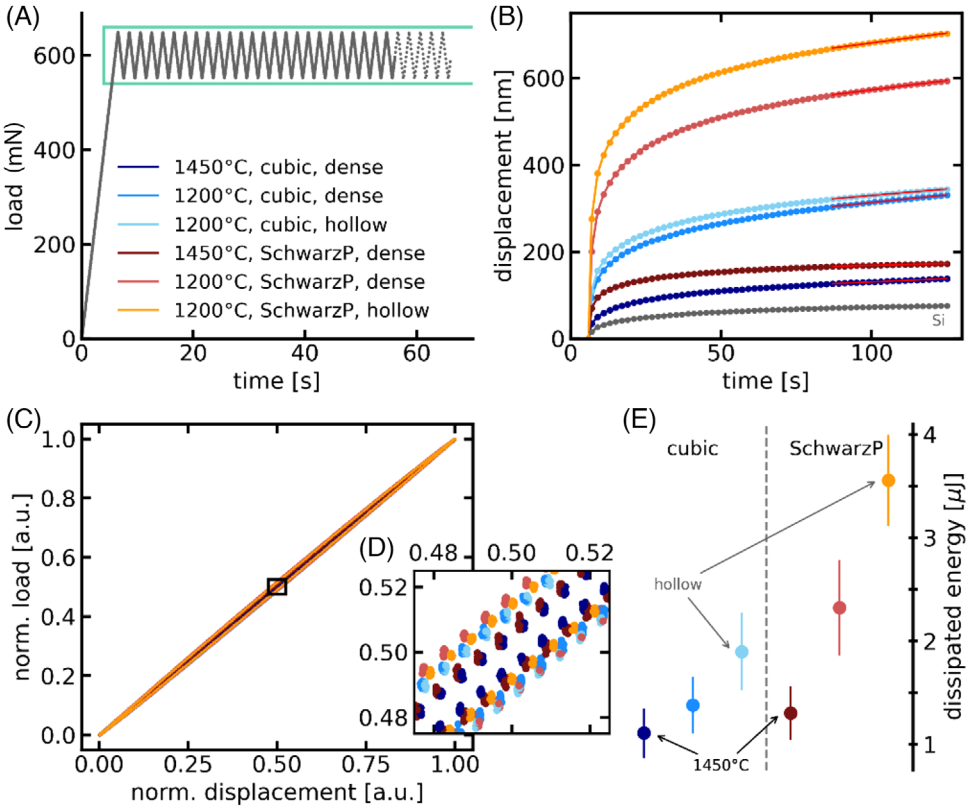

FIGURE 5 Quantification of mechanical response by periodic creep tests. (Panel A) Load protocol as a function of time consisting of a linear increase up to 600 mN followed by a hold section, with 600 zigzag cycles of 50 mN amplitude and finally a linear decrease to zero load (not depicted). (Panel B) Average displacement response connected to the hold section indicated by light green box in Panel A as a function of time for various microblocks. Red lines indicate linear fitting results over the final 20 cycles of the hold section. Gray data visualize the response from the Si reference material. (Panel C) Normalized load as a function of normalized displacement for the final 20 cycles of the hold section after subtraction of the linear contribution indicated in Panel B. (Panel D) Magnified representation of data within the black square in Panel C. (Panel E) Dissipated energy based on the integrated area between the data curves plotted in C with bars reflecting the standard deviation of the data sets. The legend in Panel A is applicable to all panels of this figure.

material, SchwarzP design). Indeed, surfaces of deformed microblocks, especially those from lower sintering temperatures, show morphologies that are atypical for ceramics. Figures 3 and 4 reveal clear morphological evidence for local plastic deformation. Arrested cracks are observed in SEM micrographs in more hollow structures (see Figure 4). Based on the observations across the different structures and processing histories, both structural and microstructural origins for energy dissipation must be considered. Structural dissipation arises due to the different designs of microblocks and line packing, whereas microstructural dissipation emerges at lower sintering temperatures.

In Figure 6, we plot the dissipated energy deduced from cyclic mechanical compression against the inverse packing fraction of microblocks sintered at 1200°C. The packing fraction is defined as the volume of a microblock's material per volume of a cubic microblock of identical outer dimensions. A correlation is observed as suggested by the red line that serves as a guide to the eye, which can be motivated by the details of the printed microblocks: As the printed material density is homogeneous in out-of-plane direction, the packing fraction can be written as $\rho_f = A \times h/V_0$, where h is the height of a microblock, V_0 is the volume of the cube enclosing the specimens, and A is the contact surface, assuming that all material is aligned in vertical stacks below the contact area. For dense microblocks, A is assumed as the full squared top-surface for cubic microblocks, and as the sum of the area of the four columns of the SchwarzP microblocks. For hollow microblocks, the contact area is calculated from the percentage representing the line density and the according contact area of the dense microblocks. Both h and V_0 are the same in all considered cases. Therefore, the inverse packing fraction is expected to be directly proportional to the applied stress, $\sigma = F/A$, because at the same applied force, a larger stress is transferred to the structures. This gives some reasoning to the correlation observed in Figure 6, as it seems intuitive that with increasing stress, an increase in dissipated energy is gained.

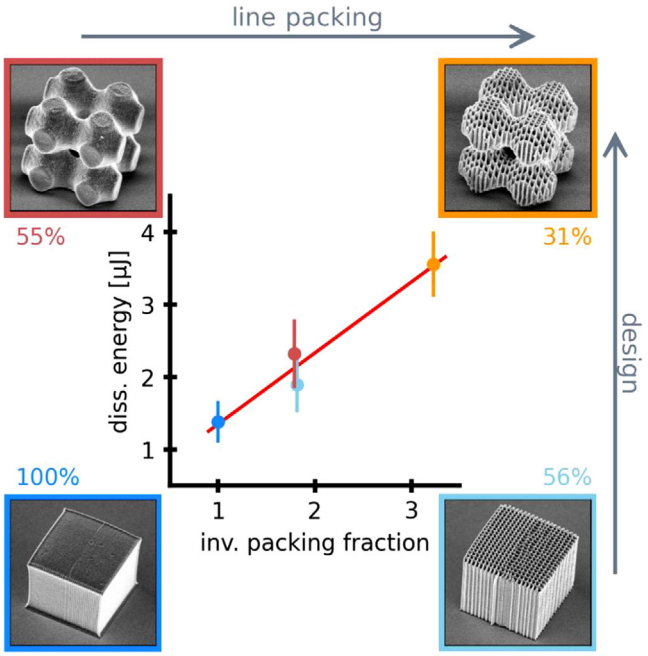

FIGURE 6 Dissipated energy as a function of inverse packing fraction for microblocks sintered at 1200°C. Packing fractions are indicated as percentages. The red line serves as a guide to the eye.

What is at the microstructural origin of energy dissipation? In conventional ceramics, mechanical dissipation and the creep signature seen in Figure 5B is normally observed at elevated temperature (e.g., around 1500°C[20]) and is associated with cationic diffusion.[21,22] At room temperature, as in the presented work, ceramic components may show observable creep due to diffusion of oxygen vacancies.[23] However, due to low diffusion rates, such behavior typically occurs on time scales of hours, that is, significantly longer than those used in this study.[24] Thus, diffusive transport is unlikely to be the origin for the here-observed mechanical dissipation behavior. Furthermore, we exclude a stress-induced phase transition toward the low-temperature monoclinic YSZ phase suggested by molecular dynamics simulations as the connected volume change is expected to be positive,[25] whereas the observed creep-like behavior shows compressive displacement accumulation of the microblocks. In addition, the here-observed deformation (~µm) exceeds expected transition-induced volumetric changes (~nm) significantly, supporting our view that energy dissipation is not dominated by a transformation to the monoclinic YSZ phase.

As the thus far considered aspects do not seem to be the primary origin of the observed dissipative behavior, we instead consider the particle size in the here presented study, which is considerably lower than for conventional ceramics. As deduced from Figure 3, grain growth of monocrystalline primary particles leads to different microstructures at the two investigated sintering temperatures. In case of the higher temperature of 1450°C, which is close to bulk zirconia sintering temperatures, initial agglomeration is followed by substantial grain growth with a resulting grain size of about 500 nm. However, at lower sintering temperature, that is, 1200°C, the primary particles presumably form polycrystalline clusters of about 100 nm in diameter, while a heterogeneous grain structure with a considerable amount of grain boundaries persists. It is this heterogeneous structure that, upon loading, allows the material to dissipate energy by disintegration—a mechanism that accounts for the difference in dissipated energy between dense microblocks sintered at 1450°C and 1200°C. While not studied systematically here, a wide temperature window is thus available, offering the perspective of tuning the damping behavior of the 2PP-AM ceramic microstructures.

Convoluted with the microstructural dissipation, the vast space of architectural design via 2PP-AM provides another pathway to enhance the damping behavior via geometry and packing fraction. In particular, the high 2PP-resolution of the order of 500 nm enables well-controlled feature sizes at a length scale that corresponds to the critical defect size of single ceramic crystallites.[26] Such filigree structures offer a second and purely geometrical mechanism for energy dissipation. In contrast, densely printed SchwarzP microblocks do not benefit from any structural features apart from grain boundaries, where these act as weakest links promoting brittle crack growth, leading to a typical deviation from theoretical strength.[27] The reduction of material per unit volume realized by designed porosity thus has a desirable impact on the mechanical response behavior of 2PP-AM ceramics as it introduces an additional mechanism for energy dissipation, an effect that is amplified by the design elements of different size, giving rise to property synergies typically attributed to metamaterials.

5 | CONCLUSION AND SUMMARY

In summary, we investigated here the mechanical response behavior of 2PP-AM YSZ-ceramic microblocks in connection to sintering temperature, line packing, and design by means of compressive loading under ambient conditions. Clear indications for microplastic dissipation are observed. This inelastic behavior is discussed in relation to energy dissipation mechanisms that are here proposed to be directly connected to the size of YSZ nanoparticles, and thus the increased number of grain boundaries, as well as printed filigree structures on the order of the critical defect size of ceramics. These two aspects contribute to a heterogeneous nano- and microstructure of the 2PP-AM YSZ-ceramic microblocks normally inaccessible to

conventional AM ceramics. Together, grain boundaries and porosity contribute to a rather forgiving ceramic material under compressive load as these two features are at the basis of sought-for dissipation mechanisms for the here presented 2PP-AM ceramic material.

ACKNOWLEDGMENTS

The authors thank Frank Meyer, CEO CeraNovis GmbH, for the generous material support. Parts of this work was performed at the electron microscopy center at BAM, with special thanks to Julian Rosalie (BAM) for conducting the TEM analysis. The authors are grateful for funds provided by the Federal Institute of Materials Research and Testing (BAM), and Birte Riechers moreover thankfully acknowledges funding provided by the European Union's Horizon Europe Framework Programme (HORIZON) under the Marie Skłodowska Curie grant agreement (No. 101063523).

ORCID

Johanna C. Sänger https://orcid.org/0009-0005-3147-5361
Birte Riechers https://orcid.org/0000-0003-4437-9844
Robert Maaß https://orcid.org/0000-0001-8329-4566
Jens Günster https://orcid.org/0000-0002-9759-0400

REFERENCES

1. Zocca A, Colombo P, Gomes CM, Günster J. Additive manufacturing of ceramics: issues, potentialities, and opportunities. J Am Ceram Soc. 2015;98(7)1983–2001. https://doi.org/10.1111/jace.13700
2. Diener S, Zocca A, Günster J. Literature review: methods for achieving high powder bed densities in ceramic powder bed based additive manufacturing. Open Ceram. 2021;8:100191. https://doi.org/10.1016/j.oceram.2021.100191
3. Cawley JD. Solid freeform fabrication of ceramics. Curr Opin Solid State Mater Sci. 1999;4(5):483–89. https://doi.org/10.1016/S1359-0286(99)00055-8
4. Lüchtenborg J, Mühler T, Léonard F, Günster J. Laser-induced slip casting (LIS)—a new additive manufacturing process for dense ceramics demonstrated with Si3N4. J Ceram Sci Technol. 2017;8(4):531–40. [Online]. Available from: https://opus4.kobv.de/opus4-bam/frontdoor/index/index/docId/43738
5. Mühler T, Gomes CM, Heinrich J, Günster J. Slurry-based additive manufacturing of ceramics. Int J Appl Ceram Technol. 2015;12(1):18–25. https://doi.org/10.1111/ijac.12113
6. Schwentenwein M, Homa J. Additive manufacturing of dense alumina ceramics. Int J Appl Ceram Technol. 2015;12(1):1–7. https://doi.org/10.1111/ijac.12319
7. Sänger JC, Pauw BR, Riechers B, Zocca A, Rosalie J, Maaß R, et al. Entering a new dimension in powder processing for advanced ceramics shaping. Adv Mater. 2022;35(8):2208653. https://doi.org/10.1002/adma.202208653
8. Bian W, Li D, Lian Q, Li X, Zhang W, Wang K, et al. Fabrication of a bio-inspired beta-tricalcium phosphate/collagen scaffold based on ceramic stereolithography and gel casting for osteochondral tissue engineering. Rapid Prototyping J. 2012;18(1):68–80. https://doi.org/10.1108/13552541211193511
9. Briscoe BJ, Khan AU, Luckham PF. Optimising the dispersion on an alumina suspension using commercial polyvalent electrolyte dispersants. J Eur Ceram Soc. 1998;18(14):2141–47. https://doi.org/10.1016/S0955-2219(98)00147-2
10. Chaim R, Levin M, Shlayer A, Estournes C. Sintering and densification of nanocrystalline ceramic oxide powders: a review. Adv Appl Ceram. 2008;107(3):159–69. https://doi.org/10.1179/174367508X297812
11. Rhodes WH. Agglomerate and particle size effects on sintering yttria-stabilized zirconia. J Am Ceram Soc. 1981;64(1):19–22. https://doi.org/10.1111/j.1151-2916.1981.tb09552.x
12. Stawarczyk B, Özcan M, Hallmann L, Ender A, Mehl A, Hämmerlet CHF. The effect of zirconia sintering temperature on flexural strength, grain size, and contrast ratio. Clin Oral Invest. 2013;17(1):269–74. https://doi.org/10.1007/s00784-012-0692-6
13. Teng X, Liu H, Huang C. Effect of Al_2O_3 particle size on the mechanical properties of alumina-based ceramics. Mater Sci Eng: A. 2007;452–453:545–51. https://doi.org/10.1016/j.msea.2006.10.073
14. Almeida HA, Bártolo PJ. Design of tissue engineering scaffolds based on hyperbolic surfaces: structural numerical evaluation. Med Eng Phys. 2014;36(8):1033–40. https://doi.org/10.1016/j.medengphy.2014.05.006 PMID:24935150
15. Restrepo S, Ocampo S, Ramírez JA, Paucar C, García C. Mechanical properties of ceramic structures based on triply periodic minimal surface (TPMS) processed by 3D printing. J Phys: Conf Ser. 2017;935(1):012036. [Online]. Available from: http://stacks.iop.org/1742-6596/935/i=1/a=012036
16. Sänger JC, Schwentenwein M, Bermejo R, Günster J. Hybridizing lithography-based ceramic additive manufacturing with two-photon-polymerization. Appl Sci. 2023;13(6):3974. [Online]. Available from: https://www.mdpi.com/2076-3417/13/6/3974
17. Zirkonoxidkeramik (ZrO_2) [cited 2024 Feb 10]. Available from: https://tkc-keramik.de/werkstoffe/oxidkeramik/zirkonoxidkeramik-zro2/
18. Srinivasan R, De Angelis RJ, Ice G, Davis BH. Identification of tetragonal and cubic structures of zirconia using synchrotron x-radiation source. J Mater Res. 1991;6(6):1287–92. https://doi.org/10.1557/JMR.1991.1287
19. Blanks KS, Kristoffersson A, Carlström E, Clegg WJ. Crack deflection in ceramic laminates using porous interlayers. J Eur Ceram Soc. 1998;18(13):1945–51. https://doi.org/10.1016/S0955-2219(98)00134-4
20. Evans PE. Creep in yttria- and scandia-stabilized zirconia. J Am Ceram Soc. 1970;53(7):365–69. https://doi.org/10.1111/j.1151-2916.1970.tb12133.x
21. Dimos D, Kohlstedt DL. Diffusional creep and kinetic demixing in yttria-stabilized zirconia. J Am Ceram Soc. 1987;70(8):531–36. https://doi.org/10.1111/j.1151-2916.1987.tb05700.x
22. Martinez-Fernandez J, Jimenez-Melendo M, Dominguez-Rodriguez A, Heuer AH. High-temperature creep of yttria-stabilized zirconia single crystals. J Am Ceram Soc. 1990;73(8):2452–56. https://doi.org/10.1111/j.1151-2916.1990.tb07612.x
23. Matsuzawa M, Horibe S. Analysis of non-elastic strain produced in zirconia ceramics. Mater Sci Eng: A. 2003;346(1):75–82. https://doi.org/10.1016/S0921-5093(02)00534-8

24. Rabe T, Kalinka G, Mieller B. Manufacturing and deformation behavior of alumina and zirconia helical springs at room temperature. J Am Ceram Soc. 2023;106(7):4261–74. https://doi.org/10.1111/jace.19085
25. Wang XZ, Liu XY, Javed A, Zhu C, Liang GY. Phase transition behavior of yttria-stabilized zirconia from tetragonal to monoclinic in the lanthanum zirconate/yttria-stabilized zirconia coupled-system using molecular dynamics simulation. J Mol Liq. 2015;207:309–14. https://doi.org/10.1016/j.molliq.2015.03.053
26. Camposilvan E, Anglada M. Size and plasticity effects in zirconia micropillars compression. Acta Mater. 2016;103:882–92. https://doi.org/10.1016/j.actamat.2015.10.047
27. Davidge RW. Mechanical properties of ceramic materials. Contemp Phys. 1969;10(2):105–24. https://doi.org/10.1080/00107516908220103

How to cite this article: Sänger JC, Riechers B, Pauw BR, Maaß R, Günster J. Microplastic response of 2PP-printed ceramics. J Am Ceram Soc. 2024;1–10. https://doi.org/10.1111/jace.19849